Proceedings of the Estonian Academy of Sciences,
2022, **71**, 1, 84–102
https://doi.org/10.3176/proc.2022.1.08
Available online at www.eap.ee/proceedings

COMPUTATIONAL MODELS FOR MULTILAYERED PLATES

Buckling analysis of angle-ply multilayered and sandwich plates using the enhanced Refined Zigzag Theory

The paper is dedicated to the 100th birthday of Professor Ülo Lepik

Matteo Sorrenti[a*], Marco Gherlone[a] and Marco Di Sciuva[b]

[a] Department of Mechanical and Aerospace Engineering, Politecnico di Torino, Corso Duca degli Abruzzi 24, 10129 Torino, Italy
[b] Former Professor of Aircraft Structures at the Department of Mechanical and Aerospace Engineering, Politecnico di Torino, Corso Duca degli Abruzzi 24, 10129 Torino, Italy

Received 11 November 2021, accepted 28 January 2022, available online 21 February 2022

Abstract. The recent enhancement of the standard Refined Zigzag Theory (RZT), herein named the enhanced Refined Zigzag Theory (en-RZT), has extended the range of applicability of the RZT to angle-ply multilayered and sandwich plates. The aim of the present investigation is to assess the numerical performances of the en-RZT for the buckling analysis of angle-ply multilayered and sandwich rectangular plates under in-plane normal loads. The linearized stability equations are obtained using the Ritz method in conjunction with the principle of virtual work, by means of Gram–Schmidt orthogonal polynomials. In order to assess the accuracy of the en-RZT, buckling loads of angle-ply laminated and sandwich plates are evaluated and compared with the numerical results available in open literature. The numerical investigation highlights the high accuracy of the en-RZT in predicting buckling loads. The study contains a parametric analysis aimed to investigate the influence of various design parameters, such as plate aspect ratio, thickness, lamina orientations, in-plane load combinations and boundary conditions on the buckling loads.

Key words: Refined Zigzag Theory, angle-ply multilayered plates, sandwich plates, warping shear functions, buckling, Ritz method.

1. INTRODUCTION

The use of multilayered composite and sandwich structures has been reported at an ever increasing rate in the last decades not only in aerospace load-carrying structures but also in automotive, marine, military and civil ones. This is due to their excellent specific properties (high strength-to-weight and stiffness-to-weight ratios), good fatigue behaviour and damping characteristics, coupled with the possibility of tailoring to optimize their structural response.

On the other hand, a crucial issue is their transverse shear deformability and through-the-thickness anisotropy. Therefore, particular attention should be paid when modelling their structural behaviour in order to accurately predict the response (in-plane displacements, transverse deflection, through-the-thickness stresses) and to achieve a reliable design.

* Corresponding author, matteo.sorrenti@polito.it

One of the main objectives of the research on structural modelling is to provide sufficiently accurate models for designers and analysts, without increasing the computational cost. Relying on relevant literature, it is worth noting that several researchers have tried to solve the three-dimensional elasticity equations for the analysis of general laminates, but this task involves mathematical difficulties in obtaining analytical solutions also for simple problems. However, three-dimensional analytical solutions for orthotropic cross-ply or sandwich plates (see [1–5]) and for anisotropic laminated plates (see [6–8]) can be used as benchmarks to verify the accuracy of axiomatic theories or approximate solutions. To the best of the authors' knowledge, few studies using three-dimensional approaches have been implemented to investigate the mechanical buckling of multilayered angle-ply structures.

It is widely recognized that the displacement-based axiomatic approaches have raised much interest in formulating accurate structural models when applied to complex problems with an affordable computational cost. According to the literature survey of Abrate and Di Sciuva [9,10], the beam/plate/shell models based on this approach can be grouped into the Equivalent Single Layer (ESL) theories and the Layer-Wise (LW) theories. The former assumes a through-the-thickness distribution of the displacement field over the whole laminate thickness. In the latter the displacement field is assumed to be independent for each layer, and it is possible to ensure the continuity of transverse stresses at the interfaces (a condition that cannot be satisfied directly in the ESL theories). Among the polynomial ESL theories used for the buckling analysis of angle-ply multilayered plates the Classical Laminate Theory (CLT), the First Order Shear Deformation Theory (FSDT) and the Reddy's Third Order Shear Deformation Theory (TSDT) should be noted. Several examples can be provided from literature. Jones et al. [11] and Sharma et al. [12] investigated the analytical solution of antisymmetrically laminated angle-ply plates using the CLT. Buckling of antisymmetric and symmetric angle-ply multilayered laminates was studied employing the FSDT by Khdeir [13] and Kabir [14], respectively. Putcha and Reddy [15] and Ni et al. [16], using the TSDT, assessed the stability analysis for anisotropic multilayered plates. Further numerical examples and comparisons were performed by Reddy [17]. Generally, depending on the plate aspect ratio, these theories are more or less accurate in predicting general quantities such as transverse displacements, fundamental frequencies, buckling loads, but are generally not accurate in predicting local quantities, i.e. thickness-wise distributions of the in-plane displacements, strain and stresses. On the other hand, the LW theories [18,19] are very accurate in predicting previous global and local quantities, but the computational cost becomes prohibitive for plates with several numbers of layers or general structures.

A good compromise between the reduced number of unknown generalized displacements of the ESL and the good accuracy of the LW theories is represented by the Zigzag Theories (ZZTs), in which the kinematic field is a superposition of a coarse (global) and a finer (local) distribution of in-plane displacements. The local improvement in the accuracy of thickness-wise distributions of the in-plane displacements and of in-plane and transverse shear stresses is due to the so-called zigzag functions. The ZZT approach allows to retain almost the same number of generalized displacements equal to that of the corresponding ESL theory, while increasing the accuracy in the estimate of the thickness-wise distributions of in-plane displacements and stresses typical of a multilayered plate. In the Di Sciuva's pioneering paper [20], the global contribution to the in-plane displacement field is represented by the FSDT, while the local enrichment is achieved by linear zigzag functions, i.e. linear step-wise functions of the thickness coordinate, whose slope allows to satisfy the continuity conditions on the transverse shear stresses.

Taking Di Sciuva's approach as a starting point, Tessler and co-workers formulated a refined zigzag theory, in the body of this paper named the standard Refined Zigzag Theory (RZT), for multilayered composite and sandwich beams [21], plates [22] and shells [23]. The interested reader can find assessment of the good performances of the standard RZT in [24–27]. Since the standard RZT requires only C^0 continuity in finite element formulation, which is very attractive from a computational point of view, many researchers have formulated and assessed various finite elements for beams/plates/shells structures [28–33].

Based on the previous examples, the standard RZT has demonstrated to be very accurate for cross-ply laminated and sandwich plates. Recently, Kreja and Sabik [34] showed that it is not possible to study multilayered angle-ply plates in which two adjacent layers have alternating orientations but the same absolute

value. Due to the derivation of zigzag functions in the standard RZT for these lamination schemes, the slope of zigzag functions is constant for each layer and, in order to satisfy the null value for these functions at the external surfaces, it results in that they are constant and null through-the-thickness. Thus, the local zigzag displacement field is null, although it has been considered a multilayered structure and from a computational point of view this leads to a singular stiffness matrix. Furthermore, the reader can easily see that in the derivation of zigzag functions for the standard RZT, the coupling effect for a general oriented layer between the two zigzag amplitudes is not considered at the level of local kinematics contribution. This coupling effect was also shown in Di Sciuva's ZZT [20] and it is present in other formulations, such as by Whitney [35] and Loredo [36].

The importance of studying general laminated structures has been testified by many authors. Among them Weaver [37] highlighted the key role represented by tailored structures in the industrial field. Moreover, it is well known by Adali et al. [38] that various lay-ups, especially the angle-ply sequences, are evaluated in the design of structures due to the uncertainties of the applied loads. More recently, experimental and numerical assessments on the stability behaviour of multilayered angle-ply plates were performed by Venkateshappa et al. [39]. A global-local higher order theory was applied by Zhen and Wanji [40] to the buckling analysis of composite and sandwich plates. Xiaohui and Zhen [41] investigated the buckling of soft-core sandwich plates with angle-ply face-sheets using third order zigzag finite elements.

In order to overcome the drawback of the standard RZT for some lay-ups highlighted by Kreja and Sabik [34] and to implement a further mathematical tool for the study of general laminates, Sorrenti and Di Sciuva [42] reformulated the standard Refined Zigzag Theory by introducing new zigzag functions in the local contribution. The newly developed model, named the enhanced RZT (en-RZT), has shown excellent predictive capabilities in [42] for the bending response of angle-ply multilayered laminate plates.

The aim of the present investigation is to assess the numerical performances of the en-RZT for the linearized buckling analysis of angle-ply multilayered and sandwich rectangular plates under in-plane normal loads.

The paper is organized as follows. Firstly, the en-RZT multilayered plate model is presented with the new zigzag functions. Based on en-RZT kinematics, the linearized equations governing the buckling of multilayered and sandwich rectangular plates under in-plane normal loads are derived using the Ritz method in conjunction with the principle of virtual work. Secondly, in order to assess the accuracy of the en-RZT, buckling loads of angle-ply laminated and sandwich plates are evaluated by means of Gram–Schmidt orthogonal polynomials and compared to the results of other refined plate models available in open literature, due to the lack of exact three-dimensional or LW mechanical buckling results for angle-ply plates. The investigation contains a parametric analysis aimed to highlight the influence of various design parameters, such as plate aspect ratio, thickness, lamina orientations, in-plane load combinations and boundary conditions on the buckling loads. Finally, some considerations on the obtained numerical results are presented.

2. MULTILAYER PLATE MODEL

2.1. Geometrical preliminaries

We consider a multilayered flat rectangular plate made of a finite number N of perfectly bonded layers. V is the volume of the plate, h denotes thickness; a_1 and a_2 are the length and width, respectively. The points of the plate are referred to an orthogonal Cartesian coordinate system defined by the vector $\mathbf{X} = \{x_i\}, (i = 1,2,3)$. The vector $\mathbf{x} = \{x_\alpha\}, (\alpha = 1,2)$ represents the set of in-plane coordinates on the reference plane, here chosen to be the middle plane of the plate, and x_3 is the coordinate normal to the reference plane, so that x_3 is defined in the range $x_3 \in [-\frac{h}{2}, +\frac{h}{2}]$, see Fig. 1. The origin of the reference frame is fixed at the centre of the middle plane of the plate, so that x_α is defined in the range $x_\alpha \in [-\frac{a_\alpha}{2}, +\frac{a_\alpha}{2}]$. In the body of the paper, also the following nondimensional coordinates will be adopted: $\xi_\alpha = \frac{2x_\alpha}{a_\alpha} \in [-1, +1]$. The thickness of each layer, as well as of the whole plate, is assumed to be constant. The material of each layer is assumed to be elastic orthotropic with a plane of elastic symmetry parallel to the reference surface and

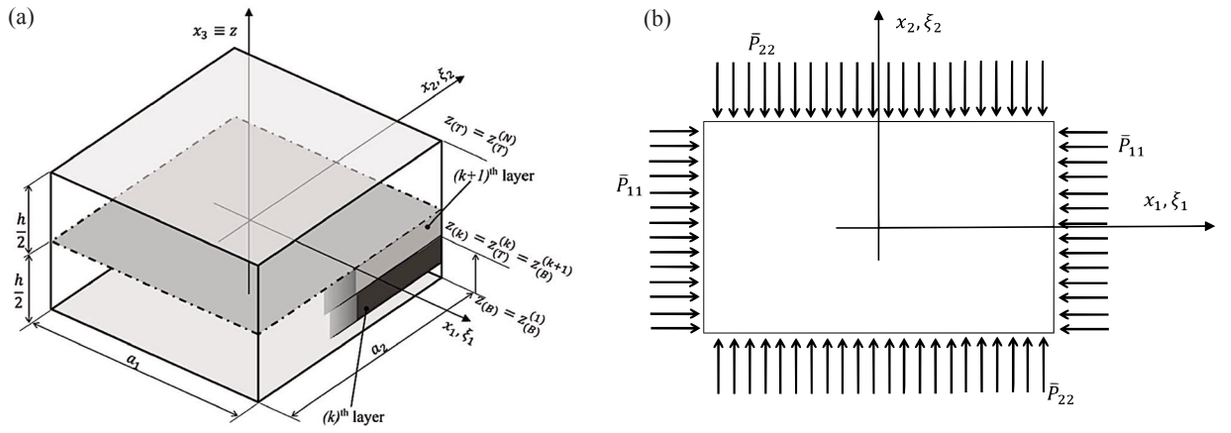

Fig. 1. General plate notation: (a) plate geometry, coordinate system and layer numbering, (b) in-plane loads.

whose principal orthotropy directions are arbitrarily oriented with respect to the in-plane reference frame. The plate is subjected to uniformly distributed in-plane normal loads for unit length, $\bar{P}_{11}$, $\bar{P}_{22}$ are applied along the edges $x_1 = \pm\frac{a_1}{2}$ and $x_2 = \pm\frac{a_2}{2}$, respectively (see Fig. 1b).

If not otherwise stated in the paper, the notation $(.)^{(k)}$ is used to indicate quantities corresponding to the k^{th} layer $(k = 1,...,N)$, whereas the notation $(.)_{(k)}$ $(k = 1,...,N-1)$ refers to $(.)$ valued for $x_3 = z_{(k)}$, i.e. at the k^{th} interface $(k = 1,...,N-1)$ between the k^{th} and the $(k+1)^{\text{th}}$ layer. In addition, we use the subscripts (B) and (T) to indicate the bottom and top surfaces of the single-layer/whole plate, respectively; specifically, $z_{(\text{B})}^{(1)} = z_{(\text{B})}$ and $z_{(\text{T})}^{(N)} = z_{(\text{T})}$ denote the coordinates of the bottom and top surfaces of the whole plate; thus, $h = z_{(\text{T})} - z_{(\text{B})}$ is the plate thickness and $h^{(k)} = z_{(k)} - z_{(k-1)} = z_{(\text{T})}^{(k)} - z_{(\text{B})}^{(k)}$ $(k = 1,2...,N)$ is the thickness of the k^{th} layer.

The symbol $(\bullet)_{,i} = \frac{\partial(\bullet)}{\partial x_i}$ refers to the derivative of the function $(\bullet)$ with respect to the coordinate x_i. In the paper, if not otherwise specified, the Einsteinian summation convention over repeated indices is adopted, with Latin indices ranging from 1 to 3, and Greek indices ranging from 1 to 2.

2.2. Enhanced RZT (en-RZT) kinematics

As usual in the axiomatic theories of plates and shells, the thickness-wise distribution of the three-dimensional displacement field is assumed a priori. Therefore, adopting this axiomatic approach, in general, we write

$$\tilde{\mathbf{d}}(\mathbf{X}) = \mathbf{Z}_d(x_3)\,\mathbf{d}(\mathbf{x}), \tag{1}$$

where

$$\tilde{\mathbf{d}}(\mathbf{X}) = \begin{Bmatrix} \tilde{u}_1(\mathbf{X}) \\ \tilde{u}_2(\mathbf{X}) \\ \tilde{u}_3(\mathbf{X}) \end{Bmatrix} = \begin{Bmatrix} \tilde{\mathbf{u}}(\mathbf{X}) \\ \tilde{u}_3(\mathbf{X}) \end{Bmatrix} \tag{2}$$

is the vector of displacement components of the generic point along the orthogonal Cartesian coordinate system $\mathbf{X} = \{x_i\}, (i = 1,2,3)$;

$$\mathbf{d}(\mathbf{x}) = \begin{Bmatrix} u_1(\mathbf{x}) \\ u_2(\mathbf{x}) \\ u_3(\mathbf{x}) \end{Bmatrix} = \begin{Bmatrix} \mathbf{u}(\mathbf{x}) \\ u_3(\mathbf{x}) \end{Bmatrix} \tag{3}$$

is the vector of the generalized displacements, independent of the x_3-coordinate, and $\mathbf{Z}_{\mathrm{d}}(x_3)$ is the matrix of the assumed thickness-wise distributions. Both $\mathbf{d}(\mathbf{x})$ and $\mathbf{Z}_{\mathrm{d}}(x_3)$ are plate/shell theory dependent.

In the kinematics of the RZT (see [42]), the transverse displacement is assumed to be constant through-the-thickness, i.e.

$$\tilde{u}_3(\mathbf{X}) = u_3(\mathbf{x}). \tag{4}$$

The in-plane kinematics is based on the superposition of a global (G) first order kinematics (which is continuous with its first derivatives with respect to the x_3-coordinate) and a local (L) layer-wise correction of the in-plane displacements (which is continuous and piecewise linear with respect to x_3, but with jumps in the first derivative at the interface between adjacent layers). Thus,

$$\tilde{\mathbf{u}}(\mathbf{X}) = \tilde{\mathbf{u}}^G(\mathbf{X}) + \tilde{\mathbf{u}}^L(\mathbf{X}), \tag{5}$$

where

$$\tilde{\mathbf{u}}^G(\mathbf{X}) = \mathbf{u}(\mathbf{x}) + x_3\boldsymbol{\theta}(\mathbf{x}), \tag{6}$$

$$\tilde{\mathbf{u}}^L(\mathbf{X}) = \boldsymbol{\phi}^{(k)}(x_3)\ \boldsymbol{\Psi}(\mathbf{x}). \tag{7}$$

The local layer-wise correction (7) vanishes on the top and bottom surfaces of the plate. Substituting Eqs (5), (6) and (7) into Eq. (1) yields

$$\mathbf{d}^T = \begin{bmatrix} u_1 & u_2 & u_3 & \theta_1 & \theta_2 & \psi_1 & \psi_2 \end{bmatrix} = \begin{bmatrix} \mathbf{u}^T & u_3 & \boldsymbol{\theta}^T & \boldsymbol{\psi}^T \end{bmatrix}, \tag{8}$$

$$\mathbf{Z}_{\mathrm{d}}^{(k)}(\mathrm{x}_3) = \begin{bmatrix} \mathbf{I} & \mathbf{0} & x_3\mathbf{I} & \boldsymbol{\phi}^{(k)} \\ \mathbf{0} & 1 & \mathbf{0} & \mathbf{0} \end{bmatrix} \tag{9}$$

with

$$\boldsymbol{\phi}^{(k)}(x_3) = \begin{bmatrix} \phi_{11}^{(k)}(x_3) & \phi_{12}^{(k)}(x_3) \\ \phi_{21}^{(k)}(x_3) & \phi_{22}^{(k)}(x_3) \end{bmatrix}; \quad \boldsymbol{\Psi}(\mathbf{x}) = \begin{Bmatrix} \psi_1(\mathbf{x}) \\ \psi_2(\mathbf{x}) \end{Bmatrix}. \tag{10}$$

In Eq. (6), $\mathbf{u}(\mathbf{x})$ and $\boldsymbol{\theta}(\mathbf{x})$ are the global uniform in-plane displacements and rotations of the normal to the reference plane about the positive x_2 and the negative x_1 directions, respectively. In Eq. (7), $\boldsymbol{\Psi}(\mathbf{x})$ denotes unknown spatial amplitudes of the $\phi^{(k)}(x_3)$ zigzag functions, the latter being the assumed piecewise linear functions through-the-thickness, vanishing on the top and bottom surfaces of the plate.

In Eq. (9) and in the body of the paper, $\mathbf{I}$ represents the identity matrix and $\mathbf{0}$ the null rectangular matrix, the dimensions of which follow from the rule of the matrix product and partitioning, and the superscript T attached to a matrix refers to transpose.

For the k^{th} layer of thickness $h^{(k)}$, the generalized zigzag functions' matrix $\phi^{(k)}(x_3)$ has the following recursive expression (see Sorrenti and Di Sciuva [42]),

$$\begin{aligned} \boldsymbol{\phi}^{(k)}(x_3) &= (x_3 - z_{(\mathrm{B})})\left(\mathbf{S}_{\mathrm{t}}^{(k)}\mathbf{G} - \mathbf{I}\ \right) + \sum_{q=1}^{k} h^{(q)}\left(\mathbf{S}_{\mathrm{t}}^{(q)} - \mathbf{S}_{\mathrm{t}}^{(k)}\right)\mathbf{G} \\ &= (x_3 - z_{(\mathrm{B})})\boldsymbol{\beta}^{(k)} + \sum_{q=1}^{k} h^{(q)}\left(\boldsymbol{\beta}^{(q)} - \boldsymbol{\beta}^{(k)}\right), \qquad (k = 1, \ldots, N), \end{aligned} \tag{11}$$

where

$$\boldsymbol{\beta}^{(k)} = \boldsymbol{\phi}_{,3}^{(k)} = \mathbf{S}_{\mathrm{t}}^{(k)}\mathbf{G} - \mathbf{I}; \quad \mathbf{G} = h\left(\sum_{k=1}^{N} h^{(k)}\mathbf{S}_{\mathrm{t}}^{(k)}\right)^{-1} \tag{12}$$

and $\mathbf{S}_{\mathrm{t}}^{(k)}$ is the matrix of the transverse shear compliance coefficients.

Eq. (11) shows that the four zigzag functions $\phi_{\alpha\pi}^{(k)}$ are a priori known piecewise linear continuous functions of x_3, vanishing on the bottom $\left(x_3 = z_{(\mathrm{B})} = -\frac{h}{2}\right)$ and top $\left(x_3 = z_{(\mathrm{T})} = +\frac{h}{2}\right)$ surfaces of the plate.

2.3. Strain-displacement relations

In analogy with Eq. (1), we put the strain-displacement relations in the following general form:

$$\tilde{\boldsymbol{\varepsilon}}(\mathbf{X}) = \mathbf{Z}_{\varepsilon}(x_3)\boldsymbol{\varepsilon}(\mathbf{x}), \tag{13}$$

where $\tilde{\varepsilon}(\mathbf{X})$ is the vector of the strain at a point of the body; $\varepsilon(\mathbf{x})$ refers to the vector of the strain measures, independent of the x_3-coordinate, and $\mathbf{Z}_{\varepsilon}(x_3)$ is the matrix giving the thickness-wise distributions of the strain components. As for Eq. (1), both $\varepsilon(\mathbf{x})$ and $\mathbf{Z}_{\varepsilon}(x_3)$ are plate/shell theory dependent. Moreover, $\varepsilon(\mathbf{x})$ are the linear strain-displacement relations. Thus, by taking into account that (see Eq. (4)) $\tilde{\varepsilon}_{33} = u_{3,3} = 0$, we can write

$$\tilde{\boldsymbol{\varepsilon}}^T = \begin{bmatrix} \tilde{\boldsymbol{\varepsilon}}_{\mathrm{p}}^T & \tilde{\boldsymbol{\gamma}}^T \end{bmatrix}, \tag{14}$$

where

$$\tilde{\boldsymbol{\varepsilon}}_p^T = \begin{bmatrix} \tilde{\varepsilon}_{11} & \tilde{\varepsilon}_{22} & \tilde{\gamma}_{12} \end{bmatrix} = \begin{bmatrix} \tilde{u}_{1,1} & \tilde{u}_{2,2} & \tilde{u}_{1,2} + \tilde{u}_{2,1} \end{bmatrix} \tag{15}$$

is the vector of the in-plane strain components, and

$$\tilde{\boldsymbol{\gamma}}^T = \begin{bmatrix} \tilde{\gamma}_{13} & \tilde{\gamma}_{23} \end{bmatrix} = \begin{bmatrix} \tilde{u}_{1,3} + u_{3,1} & \tilde{u}_{2,3} + u_{3,2} \end{bmatrix} \tag{16}$$

is the vector of the transverse shear strain components. Within the k^{th} layer, substituting the assumed in-plane displacements, Eqs (6) and (7), into Eqs (15) and (16) yields

$$\tilde{\boldsymbol{\varepsilon}}_{\mathrm{p}}^{(k)} = \boldsymbol{\varepsilon}^{(\mathrm{m})} + x_3\boldsymbol{\varepsilon}^{(\mathrm{b})} + \boldsymbol{\Phi}^{(k)}(x_3)\boldsymbol{\varepsilon}^{(\phi)}, \tag{17}$$

$$\tilde{\boldsymbol{\gamma}}^{(k)} = \boldsymbol{\gamma}^{(0)} + \boldsymbol{\phi}_{,3}^{(k)}\boldsymbol{\psi} = \boldsymbol{\gamma}^{(0)} + \boldsymbol{\beta}^{(k)}\boldsymbol{\psi}, \tag{18}$$

where

$$\boldsymbol{\varepsilon}^{(\mathrm{m})} = \begin{Bmatrix} \varepsilon_{11}^{(\mathrm{m})} \\ \varepsilon_{22}^{(\mathrm{m})} \\ \gamma_{12}^{(\mathrm{m})} \end{Bmatrix} = \begin{Bmatrix} u_{1,1} \\ u_{2,2} \\ u_{1,2} + u_{2,1} \end{Bmatrix}, \quad \boldsymbol{\varepsilon}^{(\mathrm{b})} = \begin{Bmatrix} \varepsilon_{11}^{(\mathrm{b})} \\ \varepsilon_{22}^{(\mathrm{b})} \\ \gamma_{12}^{(\mathrm{b})} \end{Bmatrix} = \begin{Bmatrix} \theta_{1,1} \\ \theta_{2,2} \\ \theta_{1,2} + \theta_{2,1} \end{Bmatrix}, \tag{19}$$

$$\boldsymbol{\varepsilon}^{(\phi)} = \begin{Bmatrix} \varepsilon_{11}^{(\phi)} \\ \varepsilon_{22}^{(\phi)} \\ \varepsilon_{12}^{(\phi)} \\ \varepsilon_{21}^{(\phi)} \end{Bmatrix} = \begin{Bmatrix} \psi_{1,1} \\ \psi_{2,2} \\ \psi_{1,2} \\ \psi_{2,1} \end{Bmatrix}, \quad \boldsymbol{\Phi}^{(k)}(x_3) = \begin{bmatrix} \phi_{11}^{(k)} & 0 & 0 & \phi_{12}^{(k)} \\ 0 & \phi_{22}^{(k)} & \phi_{21}^{(k)} & 0 \\ \phi_{21}^{(k)} & \phi_{12}^{(k)} & \phi_{11}^{(k)} & \phi_{22}^{(k)} \end{bmatrix}, \tag{20}$$

$$\boldsymbol{\gamma}^{(0)} = \begin{Bmatrix} \gamma_1^{(0)} \\ \gamma_2^{(0)} \end{Bmatrix} = \begin{Bmatrix} \theta_1 + u_{3,1} \\ \theta_2 + u_{3,2} \end{Bmatrix} = \boldsymbol{\theta} + \nabla u_3, \quad \boldsymbol{\beta}^{(k)} = \boldsymbol{\phi}_{,3}^{(k)}. \tag{21}$$

In Eq. (21), $\boldsymbol{\nabla}^T = \begin{bmatrix} (.)_{,1} & (.)_{,2} \end{bmatrix}$.

Substituting Eqs (17) and (18) into Eq. (14) and rearranging the result, within the k^{th} layer Eq. (13) reads

$$\tilde{\boldsymbol{\varepsilon}}^{(k)}(\mathbf{X}) = \begin{Bmatrix} \tilde{\boldsymbol{\varepsilon}}_{\mathrm{p}}^{(k)}(\mathbf{x}) \\ \tilde{\boldsymbol{\gamma}}^{(k)}(\mathbf{x}) \end{Bmatrix} = \begin{Bmatrix} \mathbf{Z}_{\varepsilon\mathrm{p}}^{(k)}(x_3)\boldsymbol{\varepsilon}_{\mathrm{p}}(\mathbf{x}) \\ \mathbf{Z}_{\gamma}^{(k)}(x_3)\boldsymbol{\gamma}(\mathbf{x}) \end{Bmatrix} = \mathbf{Z}_{\varepsilon}^{(k)}(x_3)\boldsymbol{\varepsilon}(\mathbf{x}), \tag{22}$$

where

$$\boldsymbol{\varepsilon}^{\mathrm{T}}(\mathbf{x}) = \begin{bmatrix} \boldsymbol{\varepsilon}_{\mathrm{p}}^{\mathrm{T}}(\mathbf{x}) & \boldsymbol{\gamma}^{\mathrm{T}}(\mathbf{x}) \end{bmatrix}; \quad \mathbf{Z}_{\varepsilon}^{(k)}(x_3) = \begin{bmatrix} \mathbf{Z}_{\varepsilon\mathrm{p}}^{(k)} & \mathbf{0} \\ \mathbf{0} & \mathbf{Z}_{\gamma}^{(k)} \end{bmatrix}, \tag{23}$$

and

$$\boldsymbol{\varepsilon}_{\mathrm{p}}^T(\mathbf{x}) = \begin{bmatrix} \boldsymbol{\varepsilon}^{(\mathrm{m})T} & \boldsymbol{\varepsilon}^{(\mathrm{b})T} & \boldsymbol{\varepsilon}^{(\phi)T} \end{bmatrix}; \quad \boldsymbol{\gamma}^T(\mathbf{x}) = \begin{bmatrix} \boldsymbol{\gamma}^{(0)T} & \boldsymbol{\psi}^T \end{bmatrix}, \tag{24}$$

$$\mathbf{Z}_{\varepsilon\mathrm{p}}^{(k)}(x_3) = \begin{bmatrix} \mathbf{I} & x_3\mathbf{I} & \boldsymbol{\Phi}^{(k)} \end{bmatrix}; \quad \mathbf{Z}_{\gamma}^{(k)} = \begin{bmatrix} \mathbf{I} & \boldsymbol{\beta}^{(k)} \end{bmatrix}. \tag{25}$$

2.4. Stress-strain relations

As usual in axiomatic plate theories, we assume $\tilde{\sigma}_{33} = 0$. According to this assumption, the reduced local elastic Hookean constitutive equations read

$$\tilde{\boldsymbol{\sigma}}_{\mathrm{p}}^{(k)} = \overline{\mathbf{Q}}_{\mathrm{p}}^{(k)} \tilde{\boldsymbol{\varepsilon}}_{\mathrm{p}}^{(k)}; \quad \tilde{\boldsymbol{\sigma}}_{\mathrm{t}}^{(k)} = \overline{\mathbf{Q}}_{\mathrm{t}}^{(k)} \tilde{\boldsymbol{\gamma}}^{(k)}. \tag{26}$$

In Eq. (26),

$$\tilde{\boldsymbol{\sigma}}_{\mathrm{p}}^{(k)T} = \begin{bmatrix} \tilde{\sigma}_{11} & \tilde{\sigma}_{22} & \tilde{\sigma}_{12} \end{bmatrix}^{(k)}, \quad \tilde{\boldsymbol{\sigma}}_{\mathrm{t}}^{(k)T} = \begin{bmatrix} \tilde{\sigma}_{13} & \tilde{\sigma}_{23} \end{bmatrix}^{(k)} \tag{27}$$

are the in-plane and transverse shear stresses; and

$$\overline{\mathbf{Q}}_{\mathrm{p}}^{(k)} = \begin{bmatrix} \overline{Q}_{11} & \overline{Q}_{12} & \overline{Q}_{16} \\ \overline{Q}_{12} & \overline{Q}_{22} & \overline{Q}_{26} \\ \overline{Q}_{16} & \overline{Q}_{26} & \overline{Q}_{66} \end{bmatrix}^{(k)}, \quad \overline{\mathbf{Q}}_{\mathrm{t}}^{(k)} = \begin{bmatrix} \overline{Q}_{44} & \overline{Q}_{45} \\ \overline{Q}_{45} & \overline{Q}_{55} \end{bmatrix}^{(k)}. \tag{28}$$

In Eq. (28), $\overline{Q}_{ij}^{(k)}(i,j=1,2,6)$ denote the transformed plane stress elastic reduced stiffness coefficients; $\overline{Q}_{ij}^{(k)}(i,j=4,5)$ refer to the transformed transverse shear elastic reduced stiffness coefficients (see Reddy [17]).

2.5. Linearized stability equations and boundary conditions

The principle of virtual work is used herein to derive the linearized stability equations and the variationally consistent boundary conditions. The principle can be stated as follows (here δ represents the variational operator):

$$\delta W_{\mathrm{int}} = \delta W_{\mathrm{inp}}, \tag{29}$$

where

$$\delta W_{\mathrm{int}} = \int_{-a_1/2}^{+a_1/2} \int_{-a_2/2}^{+a_2/2} \left\langle \tilde{\boldsymbol{\sigma}}^{(k)T} \delta \tilde{\boldsymbol{\varepsilon}}^{(k)} \right\rangle dx_1 dx_2 = \int_{-a_1/2}^{+a_1/2} \int_{-a_2/2}^{+a_2/2} \left\langle \tilde{\boldsymbol{\sigma}}_p^{(k)T} \delta \tilde{\boldsymbol{\varepsilon}}_p^{(k)} + \tilde{\boldsymbol{\sigma}}_t^{(k)T} \tilde{\boldsymbol{\gamma}}^{(k)} \right\rangle dx_1 dx_2 \tag{30}$$

is the virtual variation of the internal work given by the stresses $\tilde{\boldsymbol{\sigma}}^{(k)}$;

$$\delta W_{\mathrm{inp}} = \int_{-a_1/2}^{+a_1/2} \int_{-a_2/2}^{+a_2/2} \left(- \begin{bmatrix} \overline{P}_{11} & 0 \\ 0 & \overline{P}_{22} \end{bmatrix} \nabla u_3 \right)^T \delta \nabla u_3 dx_1 dx_2 = \int_{-a_1/2}^{+a_1/2} \int_{-a_2/2}^{+a_2/2} \left(\overline{\mathbf{P}} \nabla u_3 \right)^T \delta \nabla u_3 dx_1 dx_2 \tag{31}$$

is the virtual variation of the work done by the in-plane applied loads in the buckling mode (linearized stability equations).

It is assumed that the plate is loaded by uniformly distributed in-plane normal loads for unit length, $\overline{P}_{11}, \overline{P}_{22}$ are applied on the edges (see Fig. 1b). Moreover, it is assumed that $\overline{P}_{11}, \overline{P}_{22}$ vary neither in magnitude nor in direction during buckling.

It is known that for general laminated plates there is a bending and stretching coupling [43]; thus, it is impossible for the plate to remain flat in the pre-buckling state, as assumed by the linearized stability approach. However, as investigated by Leissa [44], Whitney [45] and later by Loughlan [46], simply supported and clamped antisymmetric laminated plates under in-plane normal loads remain flat until the buckling load is reached.

In the previous equations, an overbar denotes the prescribed value of a quantity. All other symbols have been defined above. Moreover, $\langle \bullet \rangle = \sum_{k=1}^{N} \int_{z_{(\mathrm{B})}^{(k)}}^{z_{(\mathrm{T})}^{(k)}} (\bullet) dx_3$.
Substitution of Eq. (22) into Eq. (30) yields

$$\delta W_{\mathrm{int}} = \int_{\Omega} \left(\mathbf{R}_{\mathrm{p}}^{T} \delta \boldsymbol{\varepsilon}_{\mathrm{p}} + \mathbf{R}_{\mathrm{t}}^{T} \delta \boldsymbol{\gamma} \right) d\Omega , \tag{32}$$

where

$$\mathbf{R}_{\mathrm{p}}^{T} = \left[\mathbf{N}^{T} \quad \mathbf{M}^{T} \quad \mathbf{M}^{(\phi)T} \right]; \ \mathbf{R}_{\mathrm{t}}^{T} = \left[\mathbf{T}^{T} \quad \mathbf{T}^{(\phi)T} \right]. \tag{33}$$

In Eq. (33), the following force and moment stress resultants for unit length have been introduced:

$$\left(\mathbf{N}, \mathbf{M}, \mathbf{M}^{(\phi)} \right) = \left(\begin{Bmatrix} N_{11} \\ N_{22} \\ N_{12} \end{Bmatrix}, \begin{Bmatrix} M_{11} \\ M_{22} \\ M_{12} \end{Bmatrix}, \begin{Bmatrix} M_{11}^{(\phi)} \\ M_{22}^{(\phi)} \\ M_{12}^{(\phi)} \\ M_{21}^{(\phi)} \end{Bmatrix} \right) = \left\langle \left(1, x_3, \boldsymbol{\Phi}^{(k)\mathrm{T}} \right) \tilde{\boldsymbol{\sigma}}_{\mathrm{p}}^{(k)} \right\rangle , \tag{34}$$

$$\left(\mathbf{T}, \mathbf{T}^{(\phi)} \right) = \left(\begin{Bmatrix} T_1 \\ T_2 \end{Bmatrix}, \begin{Bmatrix} T_1^{(\phi)} \\ T_2^{(\phi)} \end{Bmatrix} \right) = \left\langle \left(1, \boldsymbol{\phi}_{,3}^{(k)} \right) \tilde{\boldsymbol{\sigma}}_{\mathrm{t}}^{(k)} \right\rangle . \tag{35}$$

The plate constitutive relations of the enhanced RZT are derived by using Eqs (26) and (22) in Eqs (34) and (35), and integrating them over the plate thickness. The resulting plate constitutive relations are

$$\begin{Bmatrix} \mathbf{N} \\ \mathbf{M} \\ \mathbf{M}^{(\phi)} \end{Bmatrix} = \begin{bmatrix} \mathbf{A} & \mathbf{B} & \mathbf{A}^{(\phi)} \\ \mathbf{B} & \mathbf{D} & \mathbf{B}^{(\phi)} \\ \mathbf{A}^{(\phi)T} & \mathbf{B}^{(\phi)T} & \mathbf{D}^{(\phi)} \end{bmatrix} \begin{Bmatrix} \boldsymbol{\varepsilon}^{(\mathrm{m})} \\ \boldsymbol{\varepsilon}^{(\mathrm{b})} \\ \boldsymbol{\varepsilon}^{(\phi)} \end{Bmatrix}; \ \begin{Bmatrix} \mathbf{T} \\ \mathbf{T}^{(\phi)} \end{Bmatrix} = \begin{bmatrix} \mathbf{A}_{\mathrm{t}} & \mathbf{B}_{\mathrm{t}}^{(\phi)} \\ \mathbf{B}_{\mathrm{t}}^{(\phi)T} & \mathbf{D}_{\mathrm{t}}^{(\phi)} \end{bmatrix} \begin{Bmatrix} \boldsymbol{\gamma}^{(0)} \\ \boldsymbol{\psi} \end{Bmatrix}, \tag{36}$$

where

$$\begin{aligned} &\left(\mathbf{A}, \mathbf{B}, \mathbf{D} \right) = \left\langle \bar{\mathbf{Q}}_{\mathrm{p}}^{(k)} (1, x_3, x_3^2) \right\rangle, \ \left(\mathbf{A}^{(\phi)}, \mathbf{B}^{(\phi)}, \mathbf{D}^{(\phi)} \right) = \left\langle \left(1, x_3, \boldsymbol{\Phi}^{(k)\mathrm{T}} \right) \bar{\mathbf{Q}}_{\mathrm{p}}^{(k)} \boldsymbol{\Phi}^{(k)} \right\rangle, \\ &\left(\mathbf{A}_{\mathrm{t}}, \mathbf{B}_{\mathrm{t}}^{(\phi)} \right) = \left\langle \bar{\mathbf{Q}}_{\mathrm{t}}^{(k)} \left(1, \boldsymbol{\phi}_{,3}^{(k)} \right) \right\rangle, \quad \mathbf{D}_{\mathrm{t}}^{(\phi)} = \left\langle \boldsymbol{\phi}_{,3}^{(k)\mathrm{T}} \bar{\mathbf{Q}}_{\mathrm{t}} \boldsymbol{\phi}_{,3}^{(k)} \right\rangle . \end{aligned} \tag{37}$$

Substitution of Eqs (31) and (32) into the principle of virtual work (Eq. (29)), integrating them by parts and rearranging the various contributions, yields the two-dimensional statement of the principle of virtual work for the linearized buckling problem. Note that the initial pre-buckling state of the plate is compatible with the condition of uniform strain state.

2.6. Discrete buckling equations: Ritz method

Due to the difficulty in obtaining closed form solutions, we seek an approximate solution transforming the differential problem into an algebraic one. To perform this, the discretization is accomplished applying the principle of virtual work previously stated in conjunction with the Ritz method.

Let us expand the unknown functions in the form

$$\hat{f}(\xi_1, \xi_2) = \sum_{m=1}^{M(f)} C_m^{(f)} g_m^{(f)} (\xi_1, \xi_2) = \mathbf{g}^{(f)T} \mathbf{C}_{(f)}, \tag{38}$$

where $\hat{f}(\xi_1,\xi_2)$ denotes $\hat{u}_\alpha(\xi_1,\xi_2)$, $\hat{w}(\xi_1,\xi_2)$, $\hat{\theta}_\alpha(\xi_1,\xi_2)$ and $\hat{\psi}_\alpha(\xi_1,\xi_2)$ $(\alpha=1,2)$, respectively. In Eq. (38), $C_m^{(f)}$ are unknown generalized coordinates to be varied, and $g_m^{(f)}(\xi_1,\xi_2)$ are the approximating functions. In the Ritz method, these functions are required to be a complete set of admissible functions, i.e. at least linearly independent and satisfying the geometric (prescribed, kinematic) boundary conditions (see Di Sciuva and Sorrenti [47] for further details). Appendix A provides details of the admissible functions used in this work.

Thus, by taking Eq. (38) into account, Eqs (8), (9), (23), (24) yield

$$\mathbf{d}=\begin{Bmatrix}u_1\\u_2\\\theta_1\\\theta_2\\\psi_1\\\psi_2\\w\end{Bmatrix}=\begin{bmatrix}\mathbf{g}^{u_1T}&\mathbf{0}&\mathbf{0}&\mathbf{0}&\mathbf{0}&\mathbf{0}&\mathbf{0}\\\mathbf{0}&\mathbf{g}^{u_2T}&\mathbf{0}&\mathbf{0}&\mathbf{0}&\mathbf{0}&\mathbf{0}\\\mathbf{0}&\mathbf{0}&\mathbf{g}^{\theta_1T}&\mathbf{0}&\mathbf{0}&\mathbf{0}&\mathbf{0}\\\mathbf{0}&\mathbf{0}&\mathbf{0}&\mathbf{g}^{\theta_2T}&\mathbf{0}&\mathbf{0}&\mathbf{0}\\\mathbf{0}&\mathbf{0}&\mathbf{0}&\mathbf{0}&\mathbf{g}^{\psi_1T}&\mathbf{0}&\mathbf{0}\\\mathbf{0}&\mathbf{0}&\mathbf{0}&\mathbf{0}&\mathbf{0}&\mathbf{g}^{\psi_2T}&\mathbf{0}\\\mathbf{0}&\mathbf{0}&\mathbf{0}&\mathbf{0}&\mathbf{0}&\mathbf{0}&\mathbf{g}^{wT}\end{bmatrix}\begin{Bmatrix}\mathbf{C}_{u_1}\\\mathbf{C}_{u_2}\\\mathbf{C}_{\theta_1}\\\mathbf{C}_{\theta_2}\\\mathbf{C}_{\psi_1}\\\mathbf{C}_{\psi_2}\\\mathbf{C}_w\end{Bmatrix}, \tag{39}$$

$$\mathbf{e}=\begin{Bmatrix}\hat{\boldsymbol{\varepsilon}}_m\\\hat{\boldsymbol{\varepsilon}}_b\\\hat{\boldsymbol{\varepsilon}}_\phi\\\hat{\boldsymbol{\gamma}}^{(0)}\\\boldsymbol{\psi}\end{Bmatrix}=\begin{bmatrix}\mathbf{g}_{,1}^{u_1T}&\mathbf{0}&\mathbf{0}&\mathbf{0}&\mathbf{0}&\mathbf{0}&\mathbf{0}\\\mathbf{0}&\mathbf{g}_{,2}^{u_2T}&\mathbf{0}&\mathbf{0}&\mathbf{0}&\mathbf{0}&\mathbf{0}\\\mathbf{g}_{,2}^{u_2T}&\mathbf{g}_{,1}^{u_1T}&\mathbf{0}&\mathbf{0}&\mathbf{0}&\mathbf{0}&\mathbf{0}\\\mathbf{0}&\mathbf{0}&\mathbf{g}_{,1}^{\theta_1T}&\mathbf{0}&\mathbf{0}&\mathbf{0}&\mathbf{0}\\\mathbf{0}&\mathbf{0}&\mathbf{0}&\mathbf{g}_{,2}^{\theta_2T}&\mathbf{0}&\mathbf{0}&\mathbf{0}\\\mathbf{0}&\mathbf{0}&\mathbf{g}_{,2}^{\theta_1T}&\mathbf{g}_{,1}^{\theta_2T}&\mathbf{0}&\mathbf{0}&\mathbf{0}\\\mathbf{0}&\mathbf{0}&\mathbf{0}&\mathbf{0}&\mathbf{g}_{,1}^{\psi_1T}&\mathbf{0}&\mathbf{0}\\\mathbf{0}&\mathbf{0}&\mathbf{0}&\mathbf{0}&\mathbf{0}&\mathbf{g}_{,1}^{\psi_2T}&\mathbf{0}\\\mathbf{0}&\mathbf{0}&\mathbf{0}&\mathbf{0}&\mathbf{g}_{,2}^{\psi_1T}&\mathbf{0}&\mathbf{0}\\\mathbf{0}&\mathbf{0}&\mathbf{0}&\mathbf{0}&\mathbf{0}&\mathbf{g}_{,2}^{\psi_2T}&\mathbf{0}\\\mathbf{0}&\mathbf{0}&\mathbf{g}^{\theta_1T}&\mathbf{0}&\mathbf{0}&\mathbf{0}&\mathbf{g}_{,1}^{wT}\\\mathbf{0}&\mathbf{0}&\mathbf{0}&\mathbf{g}^{\theta_2T}&\mathbf{0}&\mathbf{0}&\mathbf{g}_{,2}^{wT}\\\mathbf{0}&\mathbf{0}&\mathbf{0}&\mathbf{0}&\mathbf{g}^{\psi_1T}&\mathbf{0}&\mathbf{0}\\\mathbf{0}&\mathbf{0}&\mathbf{0}&\mathbf{0}&\mathbf{0}&\mathbf{g}^{\psi_2T}&\mathbf{0}\end{bmatrix}\begin{Bmatrix}\mathbf{C}_{u_1}\\\mathbf{C}_{u_2}\\\mathbf{C}_{\theta_1}\\\mathbf{C}_{\theta_2}\\\mathbf{C}_{\psi_1}\\\mathbf{C}_{\psi_2}\\\mathbf{C}_w\end{Bmatrix}. \tag{40}$$

In compact matrix format

$$\mathbf{d}=\mathbf{G}\mathbf{C}, \tag{41}$$

$$\mathbf{e}=\mathbf{G}_\nabla\mathbf{C}. \tag{42}$$

Substituting this realation into Eqs (30) and (31) yields

$$\delta W_{\text{int}}=\delta\mathbf{C}^T\int_{-a_1/2}^{+a_1/2}\int_{-a_2/2}^{+a_2/2}\left(\mathbf{G}_\nabla^T\begin{bmatrix}\mathbf{A}&\mathbf{B}&\mathbf{A}^\phi&\mathbf{0}&\mathbf{0}\\\mathbf{B}&\mathbf{D}&\mathbf{B}^\phi&\mathbf{0}&\mathbf{0}\\\mathbf{A}^{\phi T}&\mathbf{B}^{\phi T}&\mathbf{D}^\phi&\mathbf{0}&\mathbf{0}\\\mathbf{0}&\mathbf{0}&\mathbf{0}&\mathbf{A}_t&\mathbf{B}_t^\phi\\\mathbf{0}&\mathbf{0}&\mathbf{0}&\mathbf{B}_t^{\phi T}&\mathbf{D}_t^\phi\end{bmatrix}\mathbf{G}_\nabla\right)dx_1dx_2\,\mathbf{C}=\delta\mathbf{C}^T\mathbf{K}\mathbf{C} \tag{43}$$

with

$$\mathbf{K} = \int_{-a_1/2}^{+a_1/2} \int_{-a_2/2}^{+a_2/2} \mathbf{G}_{\nabla}^{T} \begin{bmatrix} \mathbf{A} & \mathbf{B} & \mathbf{A}^{\phi} & \mathbf{0} & \mathbf{0} \\ \mathbf{B} & \mathbf{D} & \mathbf{B}^{\phi} & \mathbf{0} & \mathbf{0} \\ \mathbf{A}^{\phi T} & \mathbf{B}^{\phi T} & \mathbf{D}^{\phi} & \mathbf{0} & \mathbf{0} \\ \mathbf{0} & \mathbf{0} & \mathbf{0} & \mathbf{A}_t & \mathbf{B}_t^{\phi} \\ \mathbf{0} & \mathbf{0} & \mathbf{0} & \mathbf{B}_t^{\phi T} & \mathbf{D}_t^{\phi} \end{bmatrix} \mathbf{G}_{\nabla} dx_1 dx_2 \tag{44}$$

and

$$\delta W_{\text{inp}} = \delta \mathbf{C}_w^T \lambda \mathbf{k}_G \mathbf{C}_w = \delta \mathbf{C}^T \lambda \mathbf{K}_G \mathbf{C}, \tag{45}$$

where

$$\lambda = \bar{P}_{11}, \quad r_{11} = \frac{\bar{P}_{22}}{\bar{P}_{11}} \quad \text{and} \quad \mathbf{k}_G = \int_{-a_1/2}^{+a_1/2} \int_{-a_2/2}^{+a_2/2} \begin{bmatrix} \mathbf{g}_{,1}^{w} & \mathbf{g}_{,2}^{w} \end{bmatrix} \begin{bmatrix} 1 & 0 \\ 0 & r_{11} \end{bmatrix} \begin{bmatrix} \mathbf{g}_{,1}^{wT} \\ \mathbf{g}_{,2}^{wT} \end{bmatrix} dx_1 dx_2 \tag{46}$$

and

$$\mathbf{K}_G = \begin{bmatrix} \mathbf{0} & \mathbf{0} & \mathbf{0} & \mathbf{0} & \mathbf{0} & \mathbf{0} & \mathbf{0} \\ \mathbf{0} & \mathbf{0} & \mathbf{0} & \mathbf{0} & \mathbf{0} & \mathbf{0} & \mathbf{0} \\ \mathbf{0} & \mathbf{0} & \mathbf{0} & \mathbf{0} & \mathbf{0} & \mathbf{0} & \mathbf{0} \\ \mathbf{0} & \mathbf{0} & \mathbf{0} & \mathbf{0} & \mathbf{0} & \mathbf{0} & \mathbf{0} \\ \mathbf{0} & \mathbf{0} & \mathbf{0} & \mathbf{0} & \mathbf{0} & \mathbf{0} & \mathbf{0} \\ \mathbf{0} & \mathbf{0} & \mathbf{0} & \mathbf{0} & \mathbf{0} & \mathbf{0} & \mathbf{0} \\ \mathbf{0} & \mathbf{0} & \mathbf{0} & \mathbf{0} & \mathbf{0} & \mathbf{0} & \mathbf{k}_G \end{bmatrix} \tag{47}$$

is the geometric stiffness matrix.

Substitution of Eqs (43) and (45) into Eq. (29), taking into account that the virtual variations are arbitrary independent variations, yields the following approximate discretized buckling equations:

$$(\mathbf{K} + \lambda \mathbf{K}_G)\,\mathbf{C} = \mathbf{0}. \tag{48}$$

2.7. Boundary conditions

With reference to a rectangular plate with dimensions of a_1 and a_2 along the edges parallel to the x_1- and x_2-axes, the geometric boundary conditions (BCs) used in the numerical analysis are:

- Symmetric angle-ply plates simply supported on all edges: the boundary conditions indicated here as SS-1, read
  along the edges $x_1 = -\frac{a_1}{2}, +\frac{a_1}{2}$: $u_2 = u_3 = \theta_2 = \psi_2 = 0$,
  along the edges $x_2 = -\frac{a_2}{2}, +\frac{a_2}{2}$: $u_1 = u_3 = \theta_1 = \psi_1 = 0$;
- Antisymmetric angle-ply plates simply supported on all edges: the boundary conditions indicated here as SS-2, read
  along the edges $x_1 = -\frac{a_1}{2}, +\frac{a_1}{2}$: $u_1 = u_3 = \theta_2 = \psi_2 = 0$,
  along the edges $x_2 = -\frac{a_2}{2}, +\frac{a_2}{2}$: $u_2 = u_3 = \theta_1 = \psi_1 = 0$;
- The traction-free boundary conditions do not involve any values for the kinematic unknowns;
- The clamped boundary conditions (C) read
  along the edges $x_1 = -\frac{a_1}{2}, +\frac{a_1}{2}$: $u_1 = u_2 = u_3 = \theta_1 = \theta_2 = \psi_1 = \psi_2 = 0$;
  on the edges $x_2 = -\frac{a_2}{2}, +\frac{a_2}{2}$: $u_1 = u_2 = u_3 = \theta_1 = \theta_2 = \psi_1 = \psi_2 = 0$.

3. NUMERICAL ANALYSIS

The accuracy and reliability of the enhanced RZT (en-RZT) for the static bending response was assessed in [42]. Here the numerical investigation has been limited and performed on angle-ply multilayered and sandwich plates in order to investigate the effect of various design parameters on critical buckling loads. Due to the lack of exact three-dimensional and LW results, and for mechanical buckling of angle-ply multilayered plates available in open literature, a numerical comparison with other higher order plate theories has been made [48]. The results provided here have been obtained using the Ritz method where, according to the numerical investigation performed in [47], the converged results for the critical buckling loads have been reached with only eight orthogonal GS polynomials for both axial directions. If not otherwise specified, the normalized critical buckling load (λ_{cr}) is computed as follows:

$$\lambda_{cr} = \frac{\lambda a_1^2}{E_2 h^3}.$$

Table 1 and Table 2 report the mechanical properties and the stacking sequence, respectively, for the multilayered composite and sandwich plates considered in this numerical assessment.

3.1. Assessment of the en-RZT

In the first numerical assessment of the en-RZT, a simply supported (SS-2) antisymmetric angle-ply plate subjected to a uniaxial compressive load is considered. In Table 3 the results obtained by the en-RZT are compared with those obtained by Matsunaga [48] using a two-dimensional higher order theory. It is important to note that the higher order theory developed by Matsunaga [48] underestimates the stiffness of laminated structures with respect to the three-dimensional exact solution for bending problems. Thus, a similar behaviour can be expected for critical buckling loads as well. Table 3 reports that the en-RZT critical values are slightly higher than the reference ones. With increasing the span-to-thickness ratio, the results of the en-RZT become closer and closer to [48], demonstrating that the effect of shear deformability is less relevant but present in thin plates and verifying the accuracy of the en-RZT.

It is evident from Table 3 that the critical buckling loads for the uniaxial case are very sensitive to geometry (aspect ratio) and to fibre directions. As expected, the critical buckling load increases with decreasing the span-to-thickness ratio.

Table 1. Mechanical properties of materials

Material name	E_1/E_2	E_3/E_2	G_{LT}/E_2	G_{TT}/E_2	ν_{LT}	ν_{TT}
A	40	1	0.6	0.5	0.25	0.25
B	15	1	0.5	0.35	0.3	0.35
C (isotropic)	1	1	0.39	0.39	0.3	0.3

L – Longitudinal
T – Transversal

Table 2. Stacking sequence for laminate and sandwich plates (from bottom to top)

Laminate	Normalized thickness $h^{(k)}/h$	Lamina materials	Lamina orientations [°]
L1	0.25/0.25/0.25/0.25	A/A/A/A	(+θ/–θ/+θ/–θ)
L2	$(\frac{1}{n}/\frac{1}{n})_n$	$(B/B)_n$	$(+\theta/-\theta)_n$
L3	0.25/0.5/0.25	(B/B/B)	(+45/–45/+45)
S1	0.05/0.05/0.8/0.05/0.05	(A/A/C/A/A)	(+45/–45/0/–45/+45)
S2	0.05/0.05/0.8/0.05/0.05	(A/A/C/A/A)	(+45/–45/0/+45/–45)

Table 3. Critical buckling loads (in N/mm) for uniaxial compressive loads, laminate L1 simply supported on all edges (SS-2)

		a_1/a_2					
a_1/h	θ[°]	0.5		1		2	
		[48]	Present	[48]	Present	[48]	Present
10	30	0.1592	0.1786	0.2889	0.3381	0.7939	0.9833
	45	0.1269	0.1425	0.3134	0.3714	1.0806	1.3760
	60	0.08547	0.09378	0.2889	0.3381	1.2924	1.6228
		[48]	Present	[48]	Present	[48]	Present
20	30	0.5307	0.5512	0.1054	0.1115	0.3417	0.3751
	45	0.04114	0.04269	0.1169	0.1244	0.5078	0.5699
	60	0.02630	0.02706	0.1054	0.1115	0.6369	0.7142
		[48]	Present	[48]	Present	[48]	Present
50	30	0.009377	0.009440	0.01939	0.01959	0.06927	0.07057
	45	0.007188	0.007234	0.02174	0.02199	0.1093	0.1120
	60	0.004503	0.004525	0.01939	0.01959	0.1416	0.1452

3.2. Parametric analysis

In this section the effect of various design parameters, such as the number of layers, ply orientation, aspect ratio, boundary conditions, symmetry/asymmetry, has been investigated. For this purpose, by applying the Ritz method, the converged results for the lowest critical buckling load have been reached with eight orthogonal polynomials.

In this first example (Figs 2 and 3), the normalized buckling loads as a function of lamination angle and the number of layers are investigated. The effect of uniaxial and biaxial ($r_{11} = 1$) compressive load cases is also assessed. Since the multilayered plates are antisymmetric with respect to the reference surface, the simply supported conditions refer to the SS-2 case. The boundary conditions are the following: simply supported on all edges (SSSS); simply supported (SS-2) on two edges perpendicular to x_1-axis and the other two edges are clamped (CSCS); a fully clamped plate (CCCC). All the plates have a span-to-thickness ratio equal to 8.

As evident from Fig. 4, for a four-layered antisymmetric angle-ply ($a_1/a_2 = 1$) plate (L1) the highest compressive buckling load is reached by the fully clamped case. This is not surprising since a more constrained structure has higher buckling loads.

Let us consider the effect of aspect ratio and boundary conditions on the buckling load parameter. For this purpose we study a symmetric three-layered angle-ply plate (L3). The absolute value of the lamination angle is 45°. In Table 4 the buckling load parameters for uniaxial and biaxial compressive load cases are reported. The span-to-thickness ratio is equal to 8.

Table 4. Buckling load parameters for symmetric angle-ply rectangular plate (L3)

	$r_{11} = 0$			$r_{11} = 1$		
a_1/a_2	0.5	1	2	0.5	1	2
SFSF (SS-1)	2.444	2.044	1.369	2.118	1.774	1.254
SSSS (SS-1)	5.384	12.942	21.783	4.299	6.569	10.618
CSCS (SS-1)	9.659	14.369	21.773	8.081	8.524	11.030
CCCC	9.931	10.733	21.898	8.145	4.694	7.241

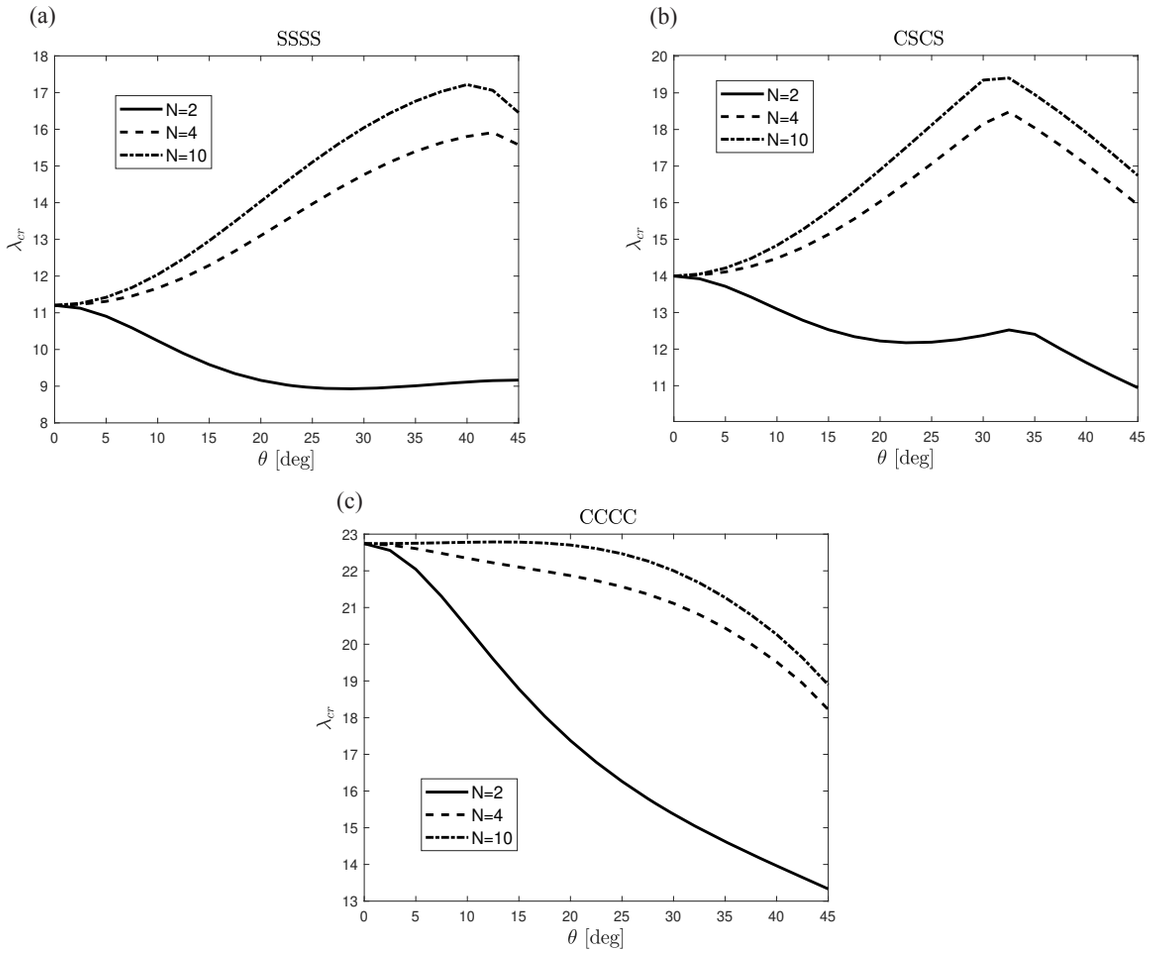

Fig. 2. Uniaxial buckling parameters for L2 squared plates.

Table 4 shows that the aspect ratio and the load combination influence the critical buckling load. As expected for both compressive in-plane loads, there is a significant reduction in critical values.

As a final comparison, the effect of the boundary conditions and the lamination scheme is investigated for sandwich plates with symmetric and antisymmetric face-sheets. For this numerical example, two cases are examined: simply supported on all edges (SS-1) and fully clamped on all edges (CCCC).

Table 5 reports the buckling load parameters for uniaxial and biaxial compressive load configurations. Figure 5 demonstrates the corresponding buckling mode shapes for uniaxial compressive case. Table 5 and Fig. 5 highlight the effect of the lamination scheme (symmetric/antisymmetric) on the value of the critical buckling parameter and on the mode shape of the plate. It is interesting to note that for the lowest buckling load value, the mode shapes do not correspond to the classical mode shape with one half-wave in each direction.

Table 5. Buckling load parameters for symmetric (S1) and antisymmetric (S2) sandwich angle-ply square plates

	Uniaxial		Biaxial	
	SSSS	CCCC	SSSS	CCCC
Sandwich S1	0.0291	0.5643	0.0240	0.2957
Sandwich S2	0.8845	0.9015	0.7105	0.7522

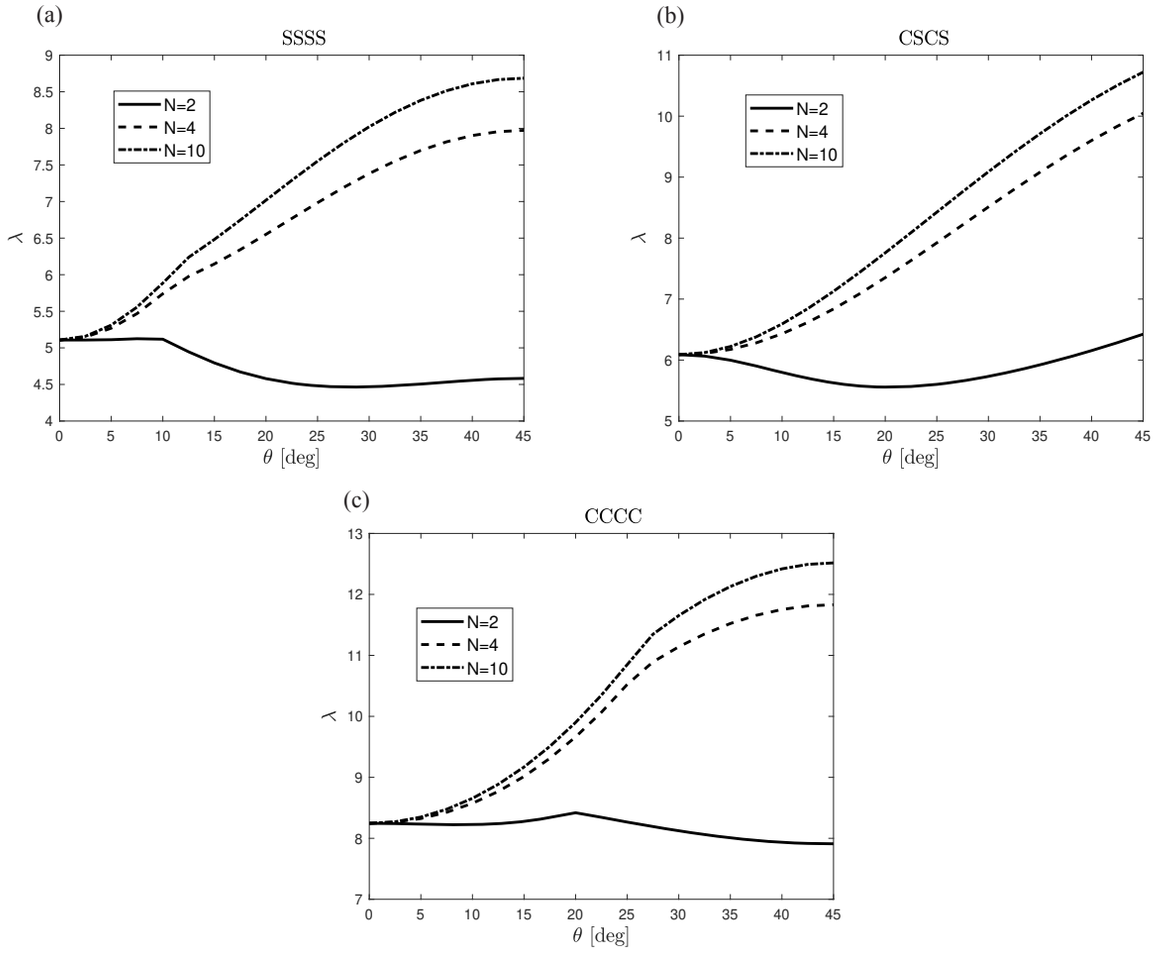

Fig. 3. Biaxial buckling parameters for L2 squared plates.

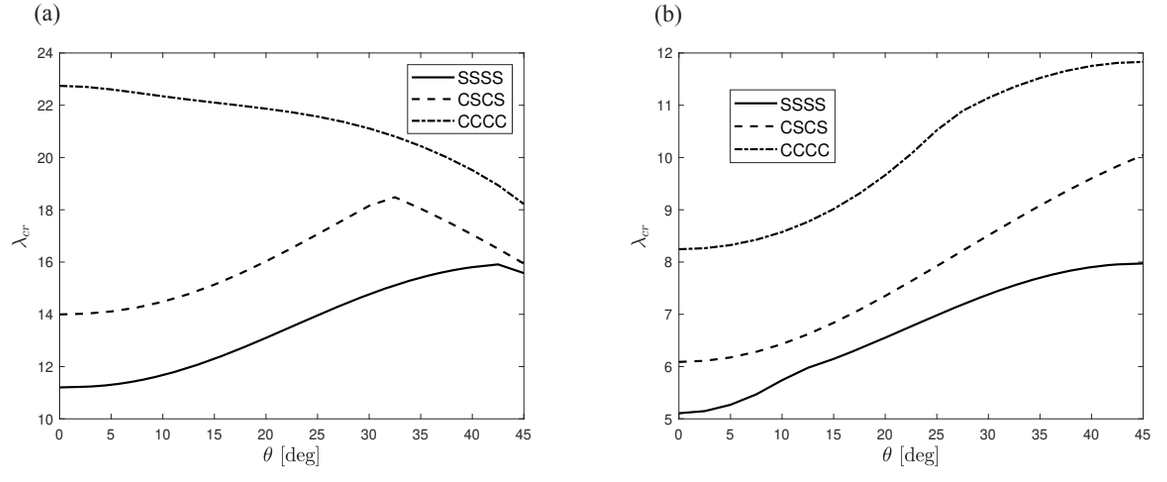

Fig. 4. Effect of BCs on buckling parameter for a) uniaxial (r_{11} = 0) and b) biaxial (r_{11} = 1) compressive loads.

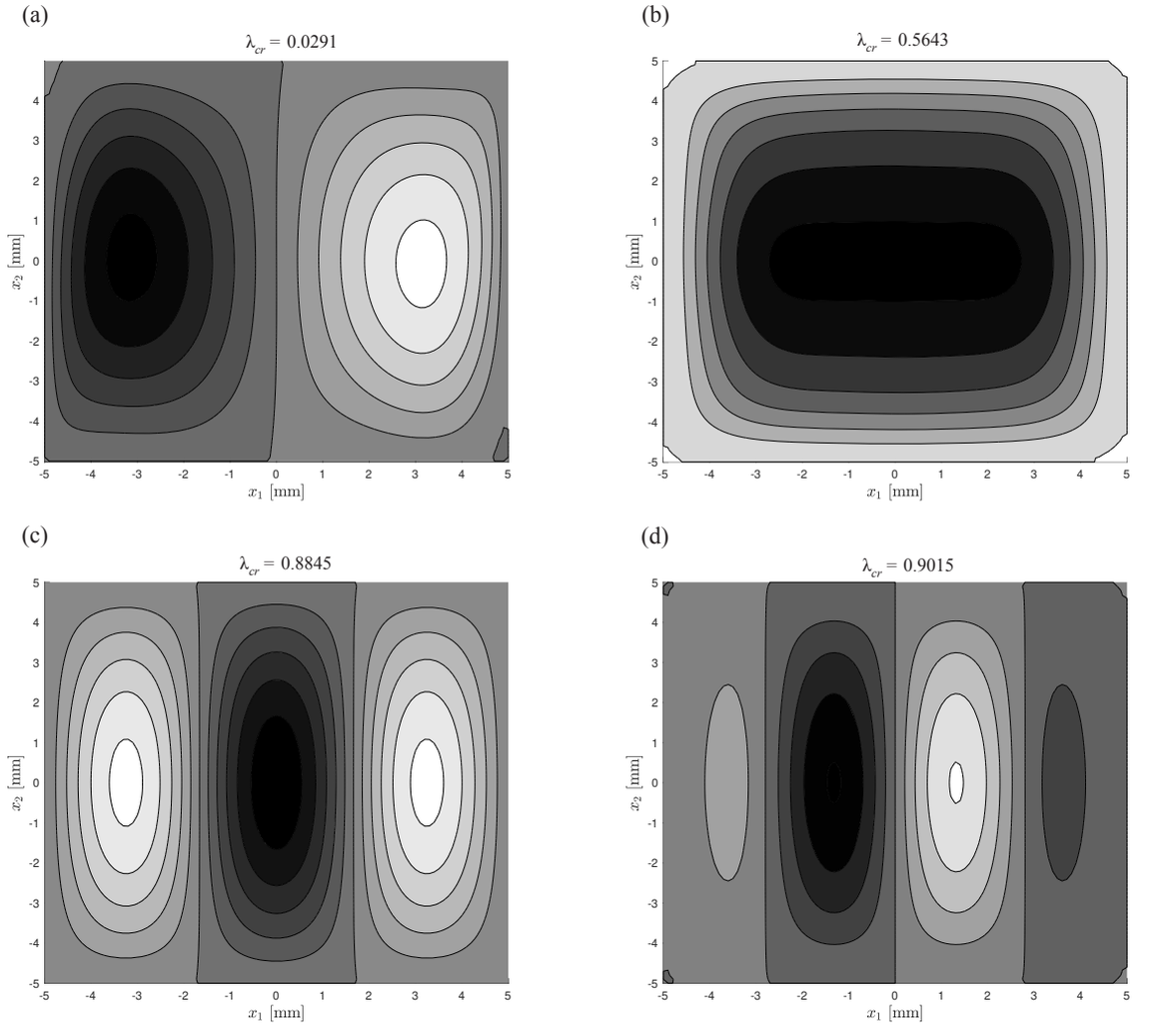

Fig. 5. Buckling mode shape for sandwich S1 (a–b) and sandwich S2 (c–d) under uniaxial compressive load.

4. CONCLUSIONS

In this paper, a linearized buckling analysis for angle-ply multilayered and sandwich plates has been performed using the recently developed enhanced Refined Zigzag Theory (en-RZT). In this theory, the enhanced local displacement field with a new set of zigzag functions allows introducing the coupling effect between the two in-plane displacements. This enhancement extends the possibility of symmetric and antisymmetric angle-ply multilayered and sandwich plates. Based on the presented results, the en-RZT is sufficiently accurate in predicting the critical buckling of various laminated angle-ply plates if compared to the other solution available in literature. In the parametric analysis, the effects of the number of layers, lamina orientations, plate geometry and boundary conditions have been thoroughly investigated by means of the approximated Ritz method. The critical buckling load for uniaxial and biaxial in-plane loads is strongly influenced by the various aspects indicated above. The en-RZT is capable of predicting and assessing each of these parameters in the design phase. The presented results computed according to the en-RZT confirm that the widely used $\theta = 45^\circ$ for the lamination scheme applied in aerospace structures is the best for carrying in-plane loads.

ACKNOWLEDGEMENT

The publication costs of this article were covered by the Estonian Academy of Sciences.

APPENDIX

The Ritz method – assumed trial functions

The Gram–Schmidt orthogonal polynomials are herein used as trial functions in the Ritz method. This linearly independent set of polynomials can also accommodate the various kinematic boundary conditions, and they present fast convergence characteristics, see [47]. Below a brief description of the procedure for constructing such polynomials is initially established for a one-dimensional problem, whereas for two-dimensional applications a simple product of one-dimensional polynomialis is used, employing the variable separation technique.

Let $g(\xi)$ be the one-dimensional Gram–Schmidt polynomial with $\xi \in [-1,1]$; the recurrence formula is

$$g_{m+1}(\xi) = (\xi - A_m) g_m(\xi) - B_m g_{m-1}(\xi),\ (m = 1,2,...) \tag{A.1}$$

with

$$A_m = \frac{\int_{-1}^{+1} \xi g_m^2(\xi) d\xi}{\int_{-1}^{+1} g_m^2(\xi) d\xi};\ B_m = \frac{\int_{-1}^{+1} g_m^2(\xi) d\xi}{\int_{-1}^{+1} g_{m-1}^2(\xi) d\xi}; \tag{A.2}$$

and

$$g_0(\xi) = 0;\ g_1(\xi) = b_1(\xi)^{\Omega_1} b_2(\xi)^{\Omega_2}, \tag{A.3}$$

where in general

$$b_i(\xi) = 0 \tag{A.4}$$

is the equation of the edge i^{th}. For the one-dimensional problem at hand,

$$b_1(\xi) = 1 + \xi \text{ and } b_2(\xi) = 1 - \xi. \tag{A.5}$$

In Eq. (A.3) the values of the exponents depend on the boundary conditions: 0 if the function does not vanish, 1 if the function vanishes (for the problem at hand see Table A.1). As mentioned above, the two-dimensional admissible functions are written as a product of one-dimensional Gram–Schmidt polynomials. Thus, for the general unknown function (38), we write

$$\hat{f}(\xi_1,\xi_2) = \sum_{p=1}^{P(f)} \sum_{r=1}^{R(f)} C_{pr}^{(f)} g_p^{(f)}(\xi_1) g_r^{(f)}(\xi_2) = \sum_{m=1}^{M(f)} C_m^{(f)} g_m^{(f)}(\xi_1,\xi_2) \tag{A. 6}$$

with

$$m = (p-1)R(f) + r. \tag{A.7}$$

The first basis function is given by

$$g_1^{(f)}(\xi_1,\xi_2) = \prod_{j=1}^{n_l} [\chi_j(\xi_1,\xi_2)]^{\Omega_j^{(f)}}, \tag{A.8}$$

where n_l gives the number of the plate edges (for quadrilateral plate, $n_l = 4$), $\chi_j(\xi_1,\xi_2) = 0$ is the equation of the j^{th} edge of the plate, the exponents Ω_j are chosen such that the geometric (prescribed) boundary condition on the edge for the function $\hat{f}(\xi_1,\xi_2)$ would be satisfied.

For example, for the square plate shown in Fig. 1, the functions $\chi_j(\xi_1,\xi_2)$ are

$$\chi_1(\xi_1,\xi_2) = (\xi_1 + 1),\ \chi_2(\xi_1,\xi_2) = (\xi_2 + 1),\ \chi_3(\xi_1,\xi_2) = (\xi_1 - 1),\ \chi_4(\xi_1,\xi_2) = (\xi_2 - 1).$$

Table A.1. Exponents for the classical geometric boundary conditions

Edge $\xi_1 = \mp 1$ SS-1	$\Omega_j^{u_1} = \Omega_j^{\theta_1} = \Omega_j^{\psi_1} = 0$ $\Omega_j^{u_2} = \Omega_j^{\theta_2} = \Omega_j^{\psi_2} = 1$
Edge $\xi_2 = \mp 1$ SS-1	$\Omega_j^{u_1} = \Omega_j^{\theta_1} = \Omega_j^{\psi_1} = 1$ $\Omega_j^{u_2} = \Omega_j^{\theta_2} = \Omega_j^{\psi_2} = 0$
Edge $\xi_1 = \mp 1$ SS-2	$\Omega_j^{u_2} = \Omega_j^{\theta_1} = \Omega_j^{\psi_1} = 0$ $\Omega_j^{u_1} = \Omega_j^{\theta_2} = \Omega_j^{\psi_2} = 1$
Edge $\xi_2 = \mp 1$ SS-2	$\Omega_j^{u_2} = \Omega_j^{\theta_1} = \Omega_j^{\psi_1} = 1$ $\Omega_j^{u_1} = \Omega_j^{\theta_2} = \Omega_j^{\psi_2} = 0$
Edge SS (for SS-1 and SS-2)	$\Omega_j^{w} = 1$
Edge F	$\Omega_j^{f} = 0$
Edge C	$\Omega_j^{f} = 1$

Table A.1 gives the exponents $\Omega_j^{(f)}$ for the classical geometric boundary condition of the RZT, according to the prescribed (geometric) values given in Section 2.7.

REFERENCES

1. Pagano, N. J. Exact solutions for composite laminates in cylindrical bending. *J. Compos. Mater*., 1969, **3**(3), 398–411.
2. Pagano, N. J. Exact solutions for rectangular bidirectional composites and sandwich plates. *J. Compos. Mater*., 1970, **4**(1), 20–34.
3. Srinivas, S. and Rao, A. K. Bending, vibration and buckling of simply supported thick orthotropic rectangular plates and laminates. *Int. J. Solids Struct*., 1970, **6**(11), 1463–1481.
4. Srinivas, S. and Rao, A. K. A three-dimensional solution for plates and laminates. *J. Franklin Inst*., 1971, **291**(6), 469–481.
5. Noor, A. K. Stability of multilayered composite plates. *Fibre Sci. Technol*., 1975, **8**(2), 81–89.
6. Noor, A. K. and Burton, W. S. Three-dimensional solutions for antisymmetrically laminated anisotropic plates. *J. Appl. Mech*., 1990, **57**(1), 182–188.
7. Noor, A. K. and Burton, W. S. Assessment of computational models for multilayered anisotropic plates. *Compos. Struct*., 1990, **14**(3), 233–265.
8. Savoia, M. and Reddy, J. N. A variational approach to three-dimensional elasticity solutions of laminated composite plates. *J. Appl. Mech*., 1992, **59**(2S), S166–S175.
9. Abrate, S. and Di Sciuva, M. Equivalent single layer theories for composite and sandwich structures: A review. *Compos. Struct*., 2017, **179**, 482–494.
10. Abrate, S. and Di Sciuva, M. Multilayer models for composite and sandwich structures. In *Comprehensive Composite Materials II* (Beaumont, P. W. R. and Zweben, C. H., eds). Elsevier, 2018, 399–425.
11. Jones, R. M., Morgan, H. S. and Whitney, J. M. Buckling and vibration of antisymmetrically laminated angle-ply rectangular plates. *J. Appl. Mech*., 1973, **40**(4), 1143–1144.
12. Sharma, S., Iyengar, N. G. R. and Murthy, P. N. Buckling of antisymmetric cross- and angle-ply laminated plates. *Int. J. Mech. Sci*., 1980, **22**(10), 607–620.
13. Khdeir, A. A. Comparison between shear deformable and Kirchhoff theories for bending, buckling and vibration of antisymmetric angle-ply laminated plates. *Compos. Struct*., 1989, **13**(3), 159–172.
14. Kabir, H. R. H. Analysis of a simply supported plate with symmetric angle-ply laminations. *Comput. Struct*., 1994, **51**(3), 299–307.
15. Putcha, N. S. and Reddy, J. N. Stability and natural vibration analysis of laminated plates by using a mixed element based on a refined plate theory. *J. Sound Vib*., 1986, **104**(2), 285–300.
16. Ni, Q.-Q., Xie, J. and Iwamoto, M. Shear buckling analysis of angle-ply laminates with higher-order shear deformation and pb-2 Ritz functions. *Sci. Eng. Compos. Mater*., 2004, **11**(2–3), 123–136.
17. Reddy, J. N. *Mechanics of Laminated Composite Plates and Shells: Theory and Analysis*. Second Edition. CRC Press, 2003.
18. D'Ottavio, M. and Carrera, E. Variable-kinematics approach for linearized buckling analysis of laminated plates and shells. *AIAA J*., 2010, **48**(9), 1987–1996.
19. Alesadi, A., Galehdari, M. and Shojaee, S. Free vibration and buckling analysis of composite laminated plates using layerwise models based on isogeometric approach and Carrera unified formulation. *Mech. Adv. Mater. Struct*., 2018, **25**(12), 1018–1032.
20. Di Sciuva, M. Geometrically nonlinear theory of multilayered plates with interlayer slips. *AIAA J*., 1997, **35**(11), 1753–1759.
21. Tessler, A., Di Sciuva, M. and Gherlone, M. Refinement of Timoshenko Beam Theory for Composite and Sandwich Beams Using Zigzag Kinematics. NASA Report. NASA/TP-2007-215086, 2007.

22. Tessler, A., Di Sciuva, M. and Gherlone, M. Refined Zigzag Theory for Laminated Composite and Sandwich Plates. NASA Report. NASA/TP-2009-215561, 2009.
23. Versino, D., Gherlone, M. and Di Sciuva, M. Four-node shell element for doubly curved multilayered composites based on the Refined Zigzag Theory. *Compos. Struct*., 2014, **118**(1), 392–402.
24. Iurlaro, L., Gherlone, M., Di Sciuva, M. and Tessler, A. Assessment of the Refined Zigzag Theory for bending, vibration, and buckling of sandwich plates: A comparative study of different theories. *Compos. Struct*., 2013, **106**, 777–792.
25. Treviso, A., Mundo, D. and Tournour, M. A C^0-continuous RZT beam element for the damped response of laminated structures. *Compos. Struct*., 2015, **131**, 987–994.
26. Iurlaro, L., Gherlone, M., Mattone, M. and Di Sciuva, M. Experimental assessment of the Refined Zigzag Theory for the static bending analysis of sandwich beams. *J. Sandw. Struct. Mater*., 2018, **20**(1), 86–105.
27. Ascione, A., Orifici, A. C. and Gherlone, M. Experimental and numerical investigation of the Refined Zigzag Theory for accurate buckling analysis of highly heterogeneous sandwich beams. *Int. J. Struct. Stab. Dyn*., 2020, **20**(07), 2050078.
28. Oñate, E., Eijo, A. and Oller, S. Simple and accurate two-noded beam element for composite laminated beams using a refined zigzag theory. *Comput. Methods Appl. Mech. Eng*., 2012, **213–216**, 362–382.
29. Di Sciuva, M., Gherlone, M., Iurlaro, L. and Tessler, A. A class of higher-order C^0 composite and sandwich beam elements based on the Refined Zigzag Theory. *Compos. Struct*., 2015, **132**, 784–803.
30. Versino, D., Gherlone, M., Mattone, M. C., Di Sciuva, M. and Tessler, A. C^0 triangular elements based on the Refined Zigzag Theory for multilayered composite and sandwich plates. *Compos. B. Eng.*, 2013, **44**(1), 218–230.
31. Gherlone, M., Versino, D. and Zarra, V. Multilayered triangular and quadrilateral flat shell elements based on the Refined Zigzag Theory. *Compos. Struct*., 2019, **233**, 111629.
32. Di Sciuva, M. and Sorrenti, M. A family of C^0 quadrilateral plate elements based on the Refined Zigzag Theory for the analysis of thin and thick laminated composite and sandwich plates. *J. Compos. Sci*., 2019, **3**(4), 100.
33. Sorrenti, M., Di Sciuva, M. and Tessler, A. A robust four-node quadrilateral element for laminated composite and sandwich plates based on Refined Zigzag Theory. *Comput. Struct*., 2021, **242**, 106369.
34. Kreja, I. and Sabik, A. Equivalent single-layer models in deformation analysis of laminated multilayered plates. *Acta Mech*., 2019, **230**(7), 2827–2851.
35. Whitney, J. M. The effect of transverse shear deformation on the bending of laminated plates. *J. Compos. Mater*., 1969, **3**(3), 534–547.
36. Loredo, A. Transverse shear warping functions for anisotropic multilayered plates. *Class. Phys*., arXiv:1211.0781.
37. Weaver, P. M. Designing composite structures: lay-up selection. *Proc. Inst. Mech. Eng. G*, 2002, **216**(2), 105–116.
38. Adali, S., Richter, A. and Verijenko, V. E. Minimum weight design of symmetric angle-ply laminates under multiple uncertain loads. *Struct. Optim*., 1995, **9**(2), 89–95.
39. Venkateshappa, S. C., Jayadevappa, S. Y. and Puttiah, P. K. W. Experimental and finite element studies on buckling of skew plates under uniaxial compression. *Sci. Eng. Compos*. *Mater*., 2015, **22**(3), 287–296.
40. Zhen, W. and Wanji, C. Buckling analysis of angle-ply composite and sandwich plates by combination of geometric stiffness matrix. *Comput. Mech*., 2007, **39**(6), 839–848.
41. Xiaohui, R. and Zhen, W. Buckling of soft-core sandwich plates with angle-ply face sheets by means of a C^0 finite element formulation. *Arch. Appl. Mech*., 2014, **84**(8), 1173–1188.
42. Sorrenti, M. and Di Sciuva, M. An enhancement of the warping shear functions of Refined Zigzag Theory. *J. Appl. Mech*., 2021, **88**(8), 084501.
43. Jones, R. M. *Mechanics of Composite Materials*. Taylor & Francis, 1999.
44. Leissa, A. W. Conditions for laminated plates to remain flat under inplane loading. *Compos. Struct*., 1986, **6**(4), 261–270.
45. Whitney, J. M. *Structural Analysis of Laminated Anisotropic Plates*. CRC Press, Lancaster, PA, 1987.
46. Loughlan, J. The influence of mechanical couplings on the compressive stability of anti-symmetric angle-ply laminates. *Compos. Struct*., 2002, **57**(1), 473–482.
47. Di Sciuva, M. and Sorrenti, M. Bending and free vibration analysis of functionally graded sandwich plates: An assessment of the Refined Zigzag Theory. *J. Sandw. Struct. Mater*., 2019, **23**(3), 760–802.
48. Matsunaga, H. Vibration and stability of angle-ply laminated composite plates subjected to in-plane stresses. *Int. J. Mech. Sci*., 2001, **43**(8), 1925–1944.

Laminaat- ja *sandwich*-tüüpi plaatide nõtkuse analüüs, kasutades modifitseeritud Zigzag teooria edasiarendusi

Matteo Sorrenti, Marco Gherlone ja Marco Di Sciuva

Kaasaegsed modifitseeritud Zigzag teooria edasiarendused (en-RZT) on laiendanud teooria rakendatavust laminaat- ja *sandwich*-tüüpi plaatidele. Käesoleva töö eesmärk on hinnata numbrilise analüüsi efektiivsust en-RZT rakendamisel tasapinnaliselt koormatud mitmekihiliste ja *sandwich*-tüüpi ristkülikplaatide korral. Rakendades Ritz'i meetodit koos

virtuaalse töö printsiibiga ja Gram-Schmidt ortogonaalseid polünoome on tuletatud lineariseeritud stabiilsuse võrrandid. En-RZT täpsuse hindamiseks on võrreldud nõtkusele vastavaid kriitilisi koormusi kirjanduseset leitud tulemustega. Läbiviidud numbrilisest analüüsist järeldub en-RZT kõrge täpsus kriitilise koormuse määramisel.

Käesolev töö sisaldab parameetrilist analüüsi, mille eesmärgiks on uurida ristkülikplaadi kuvasuhte, paksuse, kihtide materjali orientatsiooni, erinevate tasapinnaliste koormuste kombinatsioonide ja rajatingimuste mõju materjali nõtkusele ning vastavate kriitiliste koormuste väärtustele.